One-layer microfluidic device for hydrodynamic 3D self-flow-focusing operating in low flow speed

Yasaman Daghighi[1,3], Vaskar Gnyawali[2,3], Eric M. Strohm[1,3], Scott S.H. Tsai[2,3], Michael C. Kolios[1,3]
[1] Department of Physics, Ryerson University, Toronto, ON, M5B 2K3, Canada; [2] Department of Mechanical and Industrial Engineering, Ryerson University, Toronto, ON, M5B 2K3, Canada; [3] iBEST, St. Michael's Hospital, Toronto, ON, M5B 1T8, Canada

ABSTRACT

Hydrodynamic 3D flow-focusing techniques in microfluidics are categorized as (a) sheathless techniques which require high flow rates and long channels, resulting in high operating cost and high flow rates which are inappropriate for applications with flow rate limitations, and (b) sheath-flow based techniques which usually require excessive sheath flow rate to achieve hydrodynamic 3D flow-focusing. Many devices based on these principles use complicated fabrication methods to create multi-layer microchannels.

We have developed a sheath-flow based microfluidic device that is capable of hydrodynamic 3D self-flow-focusing. In this device the main flow (black ink) in a low speed, and a sheath flow, enter through two inlets and enter a 180 degree curved channel (300 × 300 μm cross-section). Main flow migrates outwards into the sheath-flow due to centrifugal effects and consequently, vertical focusing is achieved at the end of the curved channel. Then, two other sheath flows horizontally confine the main flow to achieve horizontal focusing. Thus, the core flow is three-dimensionally focused at the center of the channel at the downstream.

Using centrifugal force for 3D flow-focusing in a single-layer fabricated microchannel has been previously investigated by few groups. However, their demonstrated designs required high flow speed (>1 m/s) which is not suitable for many applications that live biomedical specie are involved. Here, we introduce a new design which is operational in low flow speed (<0.05 m/s) and is suitable for applications involving live cells. This microfluidic device can be used in detecting, counting and isolating cells in many biomedical applications.

Keywords: Microfluidics, Hydrodynamic 3D self-flow-focusing, Sheath-flow based, One-layer Fabrication, flow cytometry, cancer cell detection

1. INTRODUCTION

Flow cytometry has become a common method of providing quantitative and qualitative analysis of various types/sizes of cells or particles in rapid assays[1]. Flow cytometry is extensively used for biomedical studies (e.g. DNA content of each single cell[2–5]), clinical laboratories (e.g. Immunology clinical hematology laboratory), medical applications (e.g. immunophenotyping of urine or whole blood), and new techniques for early stage diagnosing fatal disease (such as HIV[6,7], Leukemia[8–10], and breast cancer metastasis tumors[11]).

Inside a typical flow cytometer[12], the sample (cells or particles) is drawn into the system associated with sheath flows. Before the sample pass through an interrogation point, it is preferred to be three-dimensionally (3D) focused to form a single-file stream to let the cells or particles individually travel to the downstream. Hence, hydrodynamic 3D-focusing systems are considered as the main component of such flow cytometers. Efficiency, precision, and controllability along with the manufacturing cost are important parameters in designing and testing an appropriate hydrodynamic 3D-fluid-focusing device. However, the conventional bench-top flow cytometers are currently expensive with bulky size and require considerable amount of sample and reagents to conduct the tests and provide results. Considering the substantial growth in application of flow cytometers there is a huge demand to overcome the limitations of these devices.

Microfluidic techniques have shown promising improvement in many biomedical related fields[13–17]. High efficiency micro-mixers[18–21], tunable micro-pumps[22]/-actuators[23,24], high performance micro-valves[25,26] are few examples of successful integration of microfluidics techniques into biomedical applications. The major advantages of using microfluidic devices is less required fluids and samples, smaller space, faster results, and lower cost. These positive factors make microfluidics a suitable approach to tackle the current limitations of conventional flow cytometry

Microfluidics, BioMEMS, and Medical Microsystems XIV, edited by Bonnie L. Gray, Holger Becker
Proc. of SPIE Vol. 9705, 970505 · © 2016 SPIE · CCC code: 1605-7422/16/$18 · doi: 10.1117/12.2212892

devices[27]–[29]. The main key for these approaches is developing a microfluidic device capable of 3D focusing of the sample for prior analysis[29],[30]. There have been significant efforts to develop such microfluidic systems and can be categorize as (a) sheathless technique and (b) sheath-flow based technique.

Sheathless techniques require high flow rates, which are inappropriate when live cells are involved in experiments, and long channels. Sheath-flow based techniques employs sheath flow to achieve hydrodynamic 3D flow-focusing. In sheath-flow based technique horizontal focusing can be obtain simply by using two sheath flows to sandwich the sample flow into the center of the channel. However, the vertical focusing is the main challenging component. Most of hydrodynamic 3D flow-focusing techniques were designed based on multi-layer fabrication of master molds[31]–[33] to achieve vertical focusing. It has been demonstrated that those designs could successfully focus the sample flow at the center of the microchannel, laterally and axially. However, the fabrication of multilayer devices is complicated and time consuming. In addition to the fact that the chance of devices variation when a new master is fabricated is higher than one-layer fabrication approaches.

Huang[34]–[39] and his research group has illustrated a 3D flow-focusing technique which only requires one-layer fabrication. They used high speed flow (>1 m/s) to reach high Dean Number[40] (centrifugal force concept) for vertical focusing in a curve and two sheath flows (with the same flow rates) for horizontal focusing. Their results showed that they can precisely control their focusing[39]. The main issue for the devices, which are designed based on dean flow, is excessive sheath flow rate are required to achieve vertical focusing (e.g. core flow rate of 52 μL/min while overall sheath flow rate is 787 μL/min). Such flow rate is not appropriate particularly when live biomedical species are the subject of the tests.

Here, we developed a hydrodynamic 3D flow-focusing microfluidic device which is a one-layered PDMS device that operates at low flow speed (<0.05 m/s). The device was fabricated using standard soft-lithography technique. Using this device, 3D self-flow-focusing is possible regardless of type, shape, compressibility, and size of the particles. The degree of focusing is adjustable by controlling the core and sheath flow rates, and focused flow is positioned always at the center of the microchannel. Our numerical and experimental results show that this microfluidic device successfully runs in low flow speed, and could be integrated into a flow cytometry setup for 3D focusing of live cells. Running the system under low flow rate will minimize shear stresses on live cells and prevents damaging the cells and deforming the shape of the cells.

2. HYDRODYNAMIC 3D SELF-FLOW-FOCUSING THEORY

The theory behind the 3D self-flow-focusing (when the device is one-layer microfluidic design) is focusing flow in two sequential steps: (step 1) using centrifugal force to achieve vertical focusing, and (step 2) using side sheath flows to obtain horizontal focusing. Employing this two-step procedure (which is schematically shown in Figure 1) the main flow could be focused at the center of the main channel.

Step 1: The main flow and first sheath flow (for vertical focusing) enter the system via inlet A and B, respectively. These two flow streams merge at plane P1 (figure 1) and as they flow inside the 180 degree curved channel, they experience the centrifugal force. Based on the Newtonian mechanics, the centrifugal force is greater as the object gets closer to the center of the curve; density and size of the object are additional important factors to determine the applied net force to the object. Thus, the main flow (which is closer to the inner wall of the curvature) experiences stronger outward force directed away from the center of rotation compared to the first sheath flow (which is closer to the outer wall curvature).

On the other hand, the outward motion of the sheath flow is limited by the outer wall of the curve; so, the sheath flow has to re-circulate along the cross section of the curve. As a result (and according to the conservation of mass and momentum laws), the main flow penetrates outwards into the sheath flow (plane P2, Figure 1); and will be replaced with the liquid of sheath flow. The re-circulation of the sheath flow forms one pair of counter-rotating vortices which covered the cross section of the curve. These vortices, called Dean Flow, are located on the top and the bottom of the penetrated main flow, and boost the penetration process. The penetration depth of the main flow into the sheath flow area increases as getting closer to the end of the curve (plane P3, Figure 1). Hence, the main flow is vertically focused in the middle plane of the curve when it reaches the plane P3.

Step 2: Two additional sheath flows are pumped to the system (via inlets C and D) to push the flow to the center of the channel and focus the main flow horizontally (plane P4, Figure 1). The already vertically-focused main flow at plane P4, is squeezed into the center-plane of the main channel, and become also horizontally focused at the downstream of the system (plane P5, Figure 1). The 3D flow which is focused at the center of the channel will then follow the main channel toward the outlet of the system.

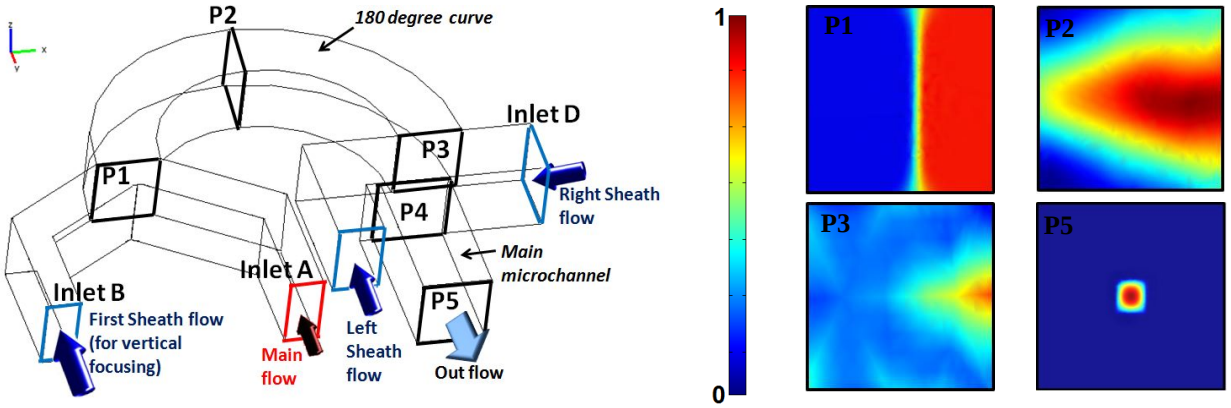

Figure 1. Schematic diagram of the hydrodynamic 3D-self-flow focusing microfluidic system. The main flow and first sheath flow (for vertical focusing) merge at the plane P1. According to the centrifugal forces in 180 degree curved channel, the main flow shrinks to the middle of the channel. This stream will be pushed to be focused in the center of the main channel using two more sheath flows (that enter the system right after plane P3). The cross sections of channels are shown by plane P1 to P5. The concentration profile at each of these planes are numerically calculated and plotted. The color bar represents the normalized concentration distribution (C/C_1).

3. NUMERICAL MODELING

3.1 Numerical Simulation and Computational Domain

Hydrodynamic 3D-self-focusing of a main flow in microchannel is numerically simulated using Comsol 3.5a. The geometry and dimensions of the computational domain are illustrated in Figure 2. The main flow and sheath flows are pumped into the device from inlets A to D. We simulated a device with 180 degree curve and obtained the optimum geometry, channel sizes, and operational flow rates. The optimum inner radius of the curve was obtained 520 µm while outer radius was 800 µm. This curved channel has constant cross section of 300 µm H × 280 µm W. Non-uniform pyramid elements covered the computational domain for more accurate solutions. The total and optimized number of meshes used for this study was 1,325,032. The specifications of microchannels used in the numerical simulations as well as the physical properties of the fluid are listed in Table 1.

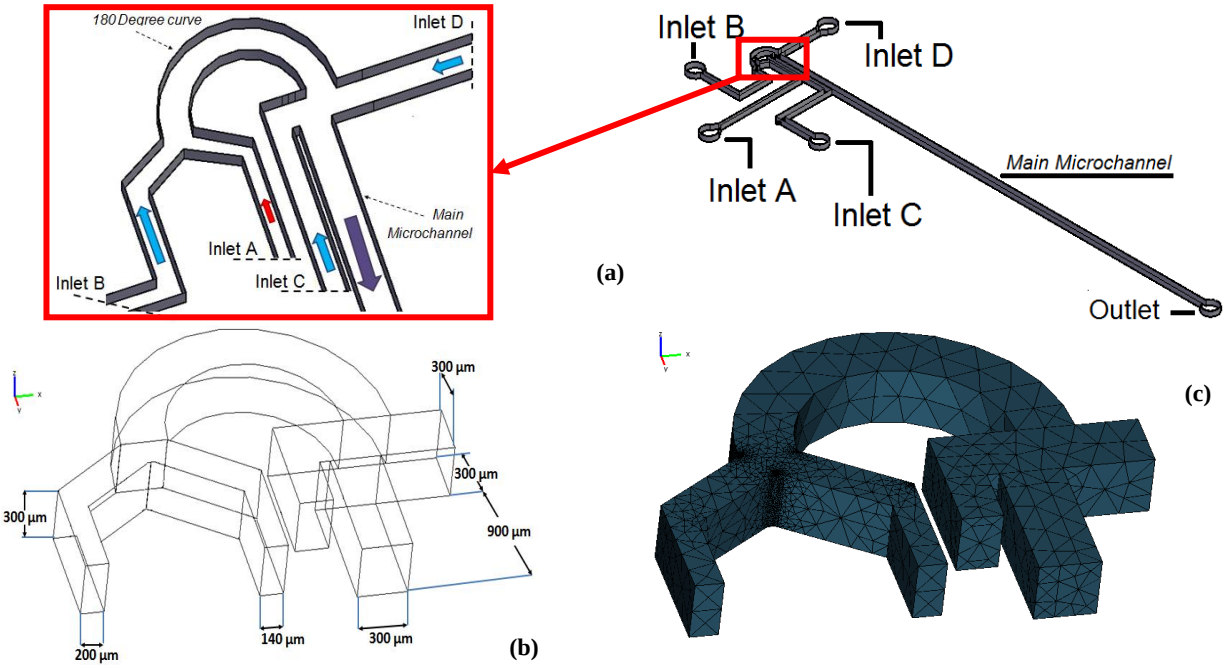

Figure 2. (a) Schematic diagram of the microchannel, (b) geometry and dimensions (c) Numerical domain covered with very coarse non-uniform pyramid mesh elements.

3.2 Governing Equations and Boundary/Initial Conditions

The governing equations for Newtonian incompressible flow in a microchannel are the mass continuity equation,

$$\nabla \cdot \vec{u} = 0, \tag{1}$$

and the Navier–Stokes equation,

$$\rho\left[\frac{\partial \vec{u}}{\partial t} + \vec{u} \cdot \vec{\nabla}\vec{u}\right] = -\vec{\nabla}p + \mu\nabla^2\vec{u} \cdot \tag{2}$$

Where, $\vec{u}$ is the velocity vector, $\nabla\vec{p}$ is the pressure gradient, μ and ρ are the viscosity and density of the fluid, respectively. The following boundary conditions were used to solve the mass and momentum equations for the simulation:

$$\vec{u} = U_{in\_k}, \qquad \text{at inlet k=A, B, C, or D} \tag{3-a}$$

$$\vec{n} \cdot \vec{\nabla}\vec{u} = 0, \qquad p = P_0, \qquad \text{at outlet} \tag{3-b}$$

$$\text{and } \vec{n} \cdot \vec{\nabla}p = 0. \qquad \text{at channel walls} \tag{3-c}$$

To determine the focus of the flow, we simulated the fluid flow equations in the microchannel, coupled with the advection-diffusion equation,

$$\frac{\partial C_i}{\partial t} + \vec{u} \cdot \vec{\nabla}C_i = D_i\nabla^2 C_i \qquad \text{i=1,..,n} \tag{4}$$

where C_i is the concentration of the fluid stream i and D_i is its diffusion coefficient. Since in the present simulation, the main flow is considered water with certain sample molar concentration at inlet A and the sheath flows at inlet B to D are considered as pure water (sample molar concentration of zero), the boundary and initial conditions for concentration equation were as follows:

$$C_{main} = 3\times10^{-3} \text{ (mol/m}^3\text{)}, \qquad \text{at inlet A} \tag{5-a}$$

$$C_{sheath} = 0 \text{ (mol/m}^3\text{)}, \qquad \text{at inlets B, C, D} \tag{5-b}$$

$$\left.\frac{\partial C_i}{\partial n}\right|_{t\geq 0s} = 0, \qquad \text{at channel walls} \tag{5-c}$$

$$C\big|_{t=0s} = 0 \qquad \text{through the microchannel} \tag{5-d}$$

To avoid the gravity effects we have considered the density of the main flow to be equal to the density of the sheath flow, and both flows have homogeneous density. The walls are not permeable to the fluid; therefore there is no fluid and concentration flux perpendicular to the microchannel walls.

Table 1. Constants used for numerical modeling

Parameters	Values		Parameters	Values
Viscosity, μ (kg/m·s)	0.9×10^{-3}		Main microchannel length, *L* (cm)	3
Density, ρ (kg/m^3)	998		Microchannel depth, *W* (μm)	300
inner diameter of curve (μm)	1040		Microchannel width, *H* (μm)	300
outer diameter of curve (μm)	1600		Curvature angle, α (*degree*)	180
Diffusion coefficient, D_i (cm^2 s^{-1})	5×10^{-9}		Molar concentration at inlet A, C_1 (mol m^{-3})	3×10^{-3}

3.3 Numerical Simulation Results

Coupling and solving equations 1 to 5 over the computational domain (Figure 2b), the fluid flow and concentration profile in the system could be three-dimensionally calculated using Comsol Multiphysics 3.5a. The main flow merged into the first sheath flow at plane P1 and followed the 180 degree curve. Once the flow reached the plane P3, the main flow is vertically focused as a result of centrifugal force. At this step, plane P3 (Figure 1), the highest concentration of the main flow is located around the middle line of plane P3. Right after plane P3, two sheath flows in different flow rates were pumped into the system. Their role is squishing the main flow into the center of the main microchannel to achieve horizontal focusing.

Figure 3 shows the numerical simulation results at plane P5 where 3D focusing is obtained. 3D flow focusing has been successfully achieved and a focused stream as small up to ~20 µm was measured when $U_{First\_Sh} = 4.2\ (cm/s)$, $U_{main\ flow} = 0.04\ (cm/s)$, $U_{Right\_Sh} = 1.4\ (cm/s)$, *and* $U_{Left\_Sh} = 1.1\ (cm/s)$ (Figure 3a). It has been demonstrated that increasing the main flow velocity keeping the sheath flow velocities constant, cause the thicker focused area; however, the main flow is still well focused in the center of plane P5 (Figure 3b). Based on the numerical results of other tests, increasing the velocity of first sheath flow (which is responsible for vertical focusing) decreased the concentration of focused area, as expected (Figure 3c).

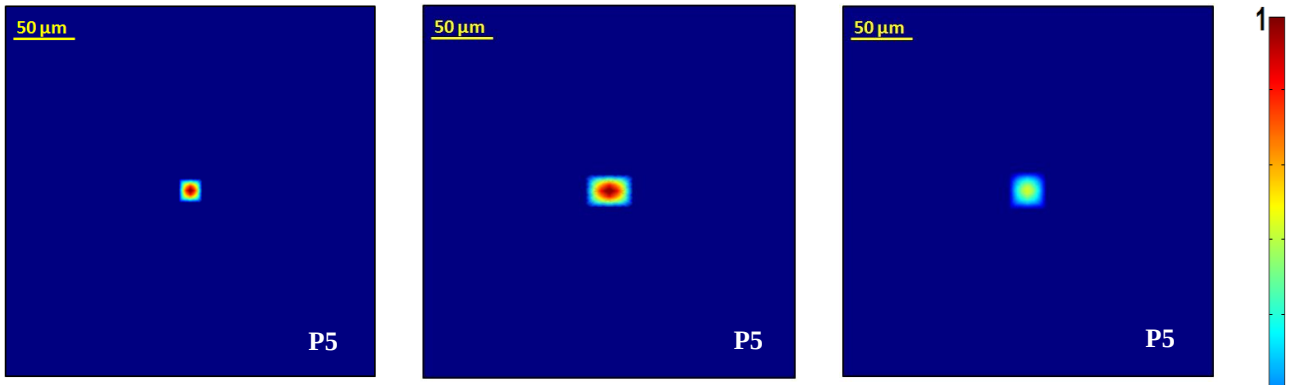

$U_{First\_Sh} = 4.2\ (cm/s)$
$U_{main\ flow} = 0.04\ (cm/s)$
$U_{Right\_Sh} = 1.4\ (cm/s)$
$U_{Left\_Sh} = 1.1\ (cm/s)$

$U_{First\_Sh} = 4.2\ (cm/s)$
$U_{main\ flow} = 0.2\ (cm/s)$
$U_{Right\_Sh} = 1.4\ (cm/s)$
$U_{Left\_Sh} = 1.1\ (cm/s)$

$U_{First\_Sh} = 8.4\ (cm/s)$
$U_{main\ flow} = 0.2\ (cm/s)$
$U_{Right\_Sh} = 1.4\ (cm/s)$
$U_{Left\_Sh} = 1.1\ (cm/s)$

Figure 3. The numerical simulation results of 3d self-flow-focusing at different flow rates. The main flow successfully focused into the center of the main microchannel at plane P5. The thickness of the focused area is a dependent factor to the injected flow rates. The color bar represents the normalized concentration distribution (C/C_1).

4. EXPERIMENTS

4.1 Microchip Fabrication

A polydimethylsiloxane (PDMS) microchip was fabricated on a glass substrate using the soft lithography method[41,42]. First, the master was prepared by spin coating the film of SU-8 2150 negative photo-resist onto a silicon wafer and then soft baked for 10 min at 65°C and then for 70 min at 95°C. A photomask bearing our microchannel geometry was placed on the top of the film, and the mask was then exposed to UV light. After post exposure baking period (25 min) and developing the mask it carefully rinsed and dried to obtain the master. Since the height of channels were 300 µm, the master cured and hard baked for 10 min at 150°C. Then, a 10:1 (w/w) mixture of PDMS polymer and curing agent was (i) poured over the master, (ii) fully degassed in a vacuum chamber, and (iii) cured at 80°C for 2 hours. The PDMS with microchannel patterns was peeled off from the master. The inlets and outlets were made by punching in holes at desired locations. Finally, the PDMS layer permanently bound onto a glass substrate. At this step, the micro-chip (with sealed microchannels) was ready to be used (Figure 4a). In our design, the microchannel's width and the depth both were 300 µm while the length of the main channel was 3cm. The tubes were connected to the four inlets to regulate the flow and there was one outlet to let the flow continually get out of the system (Figure 4b).

4.2 Experimental Setup

The fabricated micro-chip is designed to work based on hydrodynamic 3D-self-focusing. This micro-chip was connected to four independently controlled syringe pumps (Harvard Apparatus, Holliston, MA, USA) via polyethylene tubes. For this experiment, black ink solution (represents the main flow) was run into the system; while only deionized (DI) water ran in to the other three microchannels as the sheath flows. The performance of this system was tested for different flow rate combinations. The flow pattern of the main flow was recorded laterally and vertically using two CCD cameras. Each camera was connected to 10X objective lens to be capable of monitoring the flow focusing inside the main microchannel (Figure 4c). The ImageJ software was used to post-process the images and measure the thickness of the focused flow.

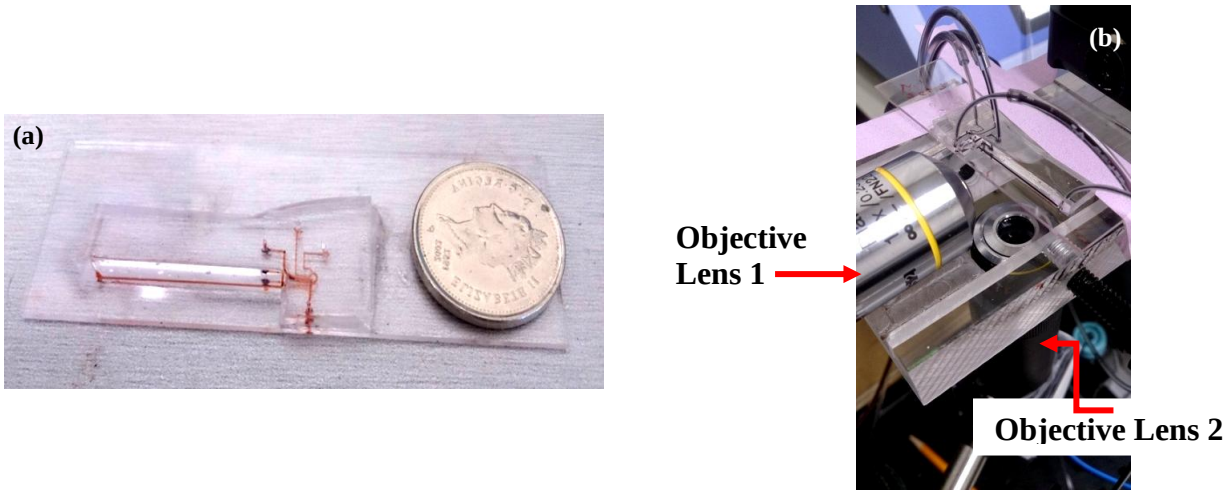

Figure 4. (a) Micro-chip and (b) the set up to visualize lateral and vertical position of the main flow. Objective lens 1 was used for lateral imaging and recording the flow pattern from side. The Objective lens 2 was used to vertically image the flow pattern from top.

4.3 Experiments

To visualize and characterize the ability of hydrodynamic 3D-self-focusing of design presented in Figure 2, the same micro-chip has been fabricated and prepared for experiments (as explained in sections 4.1 and 4.2). Black ink solution was used as sample fluid and pumped into the system trough the inlet A at the rate of 0.04 cm/s. The sheath flows are pump into the system in rate of 4.2 cm/s (through Inlet B), 1.4 cm/s (through Inlet c), and 1.1 cm/s (through Inlet D). Experimental validation of focusing performance was conducted via monitoring side-view (Figure 5a) and top-view (Figure 5b) of the flow pattern inside the microchannel. Figure 5 shows the focused flow in 1.5 cm, and 2.5 cm downstream of plane P4 (the beginning of main microchannel shown in Figure 1) in the main microchannel. As figure 5 shows the main flow was successfully focused in the center of the main microchannel, all along this channel.

The proposed system is capable of controlling the location of the main stream using different flow rate. Figure 6a and b illustrate that if $U_{First\_Sh} = 4.2\ (cm/s), U_{main\ flow} = 0.3\ (cm/s), U_{Right\_Sh} = 2.8\ (cm/s), and\ U_{Left\_Sh} = 2.0\ (cm/s)$ the 3D flow-focusing is achieved. Once the left sheath flow stops, there were no pushing force toward the center of the main microchannel, and as a result, the fluid stream got closer to the left wall (Figure 6c). The same phenomenon observes when $U_{Right\_Sh} = 0\ (cm/s), and\ U_{Left\_Sh} = 2.5\ (cm/s)$; thus the main flow follows the right wall of the main microchannel (Figure 6d). It was also shown that misbalancing the repealing forces from right sheath and left sheath could end in having the main liquid flow off the center of the main channel (Figure 6e).

The proposed device was capable of 3D-self-flow focusing of the sample or main liquid while no complicated multi-layer fabrication was required. The location of the focused flow and its thickness were tunable and sensitive to the rate of flow which was injected to the system. The main feature of the presented device was functionality of this micro-system using low flow rates. This important feature turns this device to a potential candidate for experiments where live biomedical species (e.g. cells) are involved.

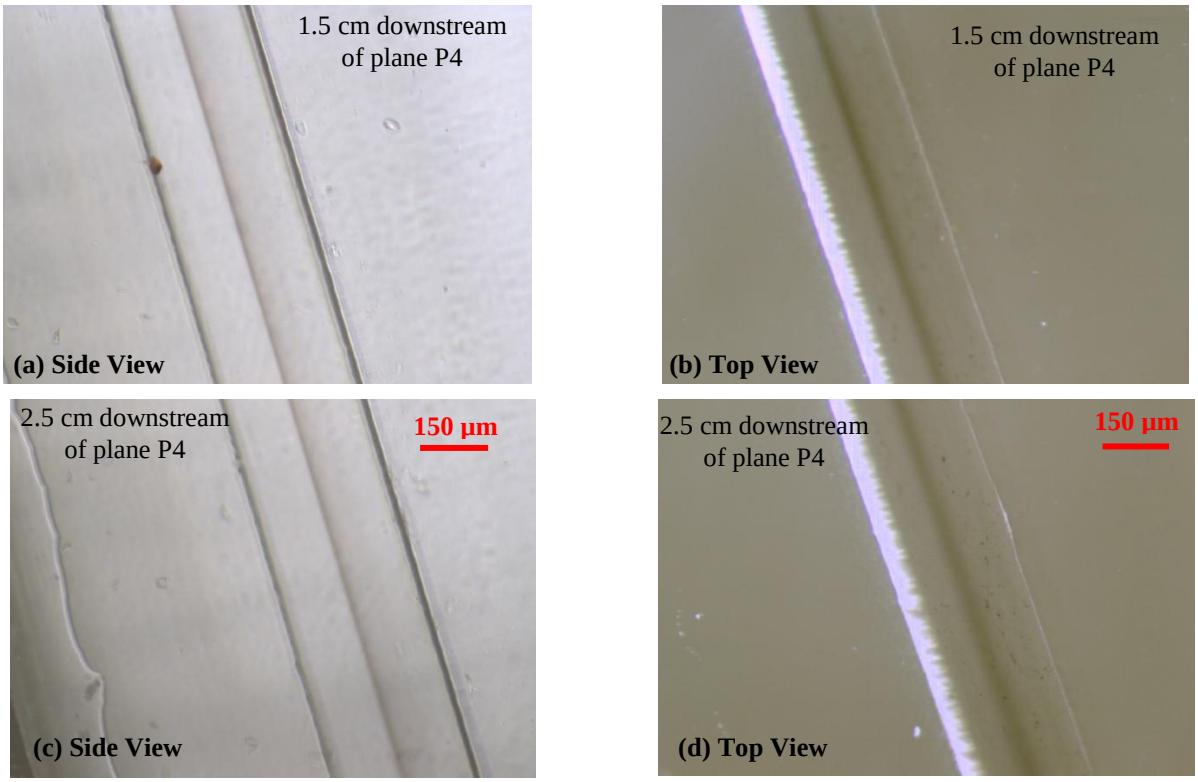

Figure 5. Our experimental results support the numerical results. We successfully could achieve 3D-focusing of main flow (black ink) inside the main microchannel at different locations. (a) side view of main microchannel at 1.5 cm downstream of plane P4, (b) top view of main microchannel at 1.5 cm downstream of plane P4, (c) side view of main microchannel at 2.5 cm downstream of plane P4, (d) top view of main microchannel at 2.5 cm downstream of plane P4.

5. DISCUSSION

Microfluidics is one of the most utilized techniques that has been integrated in many chemical and biomedical applications[43]. Recently, microfluidics has attracted much attention for developing on-chip flow cytometry components. To achieve this goal, the sample fluid must be focused to the center of the microchannel. Various microchips have been designed and developed based on hydrodynamic focusing techniques. However, most of these studies delivered sheath flows vertically and horizontally to focus the main sample to the desired location. In order to deliver the sheath flows vertically, the microchips had been fabricated using multi-layer fabrication (multi-step photolithography and assembly) procedures. Such procedures are time consuming, expensive, complicated, with high chance of variation in final product. Other methods of 3D hydrodynamic focusing which use one-layer fabrication method to make the microchip, employs inserted needle or capillary tubing routine to achieve 3D focusing. These methods are simple (compared to multi-layer fabrication techniques) but there would be a high change that two devices that were prototyped using this method are not similar.

In this study, we numerically simulated a microfluidic device capable of 3D self-flow-focusing while only requiring single-layer fabrication. The main advantages of our proposed device is its successful functionality to be used for low flow rate (<4.2 cm/s) systems. As Figure 3 shows, the focused region remains at the center of the microchannel with different flow rates. Running the device under various flow rates directly affects the area of focused flow and its concentration. Our experimental study, also, shows that the black ink was three-dimensionally focused at the center of the main microchannel. Based on Figure 5, a good 3D focusing was achieved in the system and the main flow remained focused even at very downstream of the flow. Figure 6 shows that tuning the horizontal location of the focused flow is practical and feasible just by changing the arrangement of flow rates.

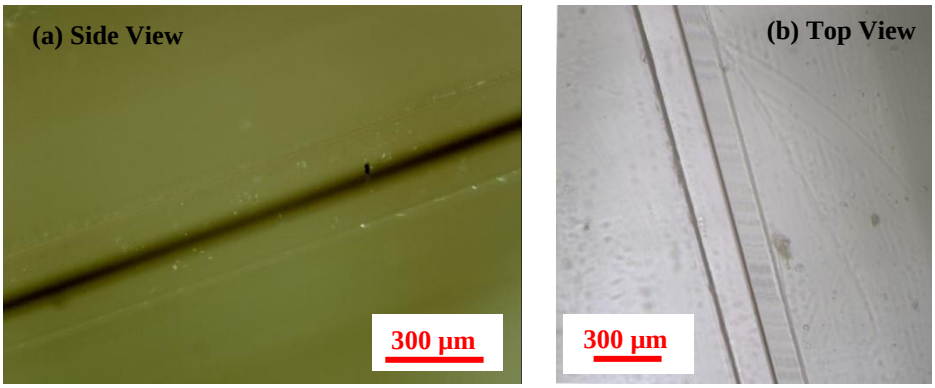

$U_{First\_Sh} = 4.2\ (cm/s), U_{main\ flow} = 0.3\ (cm/s), U_{Right\_Sh} = 2.8\ (cm/s), and\ U_{Left\_Sh} = 2.0\ (cm/s)$

$U_{First\_Sh} = 4.2\ (cm/s), U_{main\ flow} = 0.3\ (cm/s)$
$U_{Right\_Sh} = 2.8\ (cm/s), U_{Left\_Sh} = 0.0\ (cm/s)$

$U_{First\_Sh} = 4.2\ (cm/s), U_{main\ flow} = 0.3\ (cm/s)$
$U_{Right\_Sh} = 0.0\ (cm/s), U_{Left\_Sh} = 2.5\ (cm/s)$

$U_{First\_Sh} = 4.2\ (cm/s), U_{main\ flow} = 0.3\ (cm/s)$
$U_{Right\_Sh} = 1.5\ (cm/s), U_{Left\_Sh} = 2.5\ (cm/s)$

Figure 6. Controlling the location of the focused flow. (a) Side view of focused flow in the middle of main microchannel. (b)-(e) top view of main flow pattern while the flow rate changes.

6. CONCLUSION

A micro-chip design capable of hydrodynamic 3D-self-focusing of main flow was illustrated in this study. This microfluidic device is consisted of four inlets, one outlet, and a curvature angle of 180 degree (for vertical focusing). The results showed that the main stream can be successfully focused at the center of the 300×300 µm channel using low flow rates (4.2 cm/s) for hydrodynamic focusing process. This is important since the fabricated master was prepared using single-layer micro-fabrication method; thus, the 3D-self-focusing was happened in a one-layer planner microfluidic device.

Our numerical results have been experimentally verified monitoring the side and top images of the main flow in the microchannel at upstream and downstream of the flow. A narrow stream of main flow (8.4 µm H ×30.6 µm W) is achieved when the flow rate was set up at: 0.04 cm/s (inlet A) for the main flow and 4.2 cm/s (inlet B), 1.4 cm/s (inlet C), and 1.1 cm/s (inlet D) for the sheath flows. The numerical simulations reveal that using different flow rates for sheath flows we can simply adjust the thickness of main flow in lateral and vertical directions. Experiments showed that the lateral position of the main flow can be changed all over the area of main microchannel if desired.

This proposed design has a great potential to evolve as an inexpensive, reproducible, and precise flow cytometry for point-of-care clinical use and medical analyses (particularly for early stage cancer diagnosis or detecting small amount of metastatic cancer cells in blood samples).

REFERENCES

[1] Shapiro, H.M., [Practical Flow Cytometry] , 4th ed., Wiley (2003).

[2] Friedlander, M.L., Hedley, D.W., and Taylor, I.W., "Clinical and biological significance of aneuploidy in human tumours.," Journal of clinical pathology 37(9), 961–974 (1984).

[3] Joensuu, H., and Klemi, P.J., "DNA aneuploidy in adenomas of endocrine organs.," The American journal of pathology 132(1), 145–151 (1988).

[4] Duque, R.E., Andreeff, M., Braylan, R.C., Diamond, L.W., and Peiper, S.C., "Consensus review of the clinical utility of DNA flow cytometry in neoplastic hematopathology.," Cytometry 14(5), 492–496 (1993).

[5] Albro, J., Bauer, K.D., Hitchcock, C.L., and Wittwer, C.T., "Improved DNA content histograms from formalin-fixed, paraffin-embedded liver tissue by proteinase K digestion.," Cytometry 14(6), 673–678 (1993).

[6] Gadol, N., Crutcher, G.J., and Busch, M.P., "Detection of intracellular HIV in lymphocytes by flow cytometry.," Cytometry 15(4), 359–70 (1994).

[7] Barnett, D., Walker, B., Landay, A., and Denny, T.N., "CD4 immunophenotyping in HIV infection," Nature reviews. Microbiology 6(11 Suppl), S7–15 (2008).

[8] Look, A.T., Roberson, P.K., Williams, D.L., Rivera, G., Bowman, W.P., Pui, C.H., Ochs, J., Abromowitch, M., Kalwinsky, D., et al., "Prognostic importance of blast cell DNA content in childhood acute lymphoblastic leukemia.," Blood 65(5), 1079–1086 (1985).

[9] Weir, E.G., and Borowitz, M.J., "Flow cytometry in the diagnosis of acute leukemia.," Seminars in hematology 38(2), 124–138 (2001).

[10] Peters, J.M., and Ansari, M.Q., "Multiparameter flow cytometry in the diagnosis and management of acute leukemia.," Archives of pathology & laboratory medicine 135(1), 44–54 (2011).

[11] Hwu, D., Boutrus, S., Greiner, C., DiMeo, T., Kuperwasser, C., and Georgakoudi, I., "Assessment of the role of circulating breast cancer cells in tumor formation and metastatic potential using in vivo flow cytometry.," in J. Biomed. Opt. 16(4), United States, p. 40501 (2011).

[12] Davis, D., "Cell Sorting by Flow Cytometry," Flow Cytometry Principles and Applications (2007).

[13] Jiang, H., Daghighi, Y., Chon, C.H., and Li, D., "Concentrating molecules in a simple microchannel.," Journal of colloid and interface science 347(2), 324–31 (2010).

[14] Ciftlik, A.T., Lehr, H.-A., and Gijs, M. a M., "Microfluidic processor allows rapid HER2 immunohistochemistry of breast carcinomas and significantly reduces ambiguous (2+) read-outs.," Proceedings of the National Academy of Sciences of the United States of America 110(14), 5363–5368 (2013).

[15] van Midwoud, P.M., Verpoorte, E., and Groothuis, G.M.M., "Microfluidic devices for in vitro studies on liver drug metabolism and toxicity.," Integrative biology : quantitative biosciences from nano to macro 3(5), 509–521 (2011).

[16] Wong, K.H.K., Chan, J.M., Kamm, R.D., and Tien, J., "Microfluidic Models of Vascular Functions," Annual Review of Biomedical Engineering 14(1), 205–230 (2012).

[17] Daghighi, Y., and Li, D., "Numerical studies of electrokinetic control of DNA concentration in a closed-end microchannel," Electrophoresis 31(5), 868–878 (2010).

[18] Berg, T.T.V. and T.S.J.L. and M.C.E. and A. van den, "Characterization method for a new diffusion mixer applicable in micro flow injection analysis systems," Journal of Micromechanics and Microengineering 9(2), 199 (1999).

[19] Daghighi, Y., and Li, D., "Numerical study of a novel induced-charge electrokinetic micro-mixer," Analytica chimica acta 763, 28–37 (2013).

[20] Zhang, K., Mi, X.-J., and Yu, M.-Z., "Design of super-efficient mixer based on induced charge electroosmotic," Thermal Science 16(5), 1534–1538 (2012).

[21] El Moctar, A.O., Aubry, N., and Batton, J., "Electro-hydrodynamic micro-fluidic mixer.," Lab on a chip 3(4), 273–80 (2003).

[22] Rife, J.., Bell, M.., Horwitz, J.., Kabler, M.., Auyeung, R.C.., and Kim, W.., "Miniature valveless ultrasonic pumps and mixers," Sensors and Actuators A: Physical 86(1-2), 135–140 (2000).

[23] Harmon, M.E., Tang, M., and Frank, C.W., "A microfluidic actuator based on thermoresponsive hydrogels," Polymer 44(16), 4547–4556 (2003).

[24] Piyasena, M.E., Newby, R., Miller, T.J., Shapiro, B., and Smela, E., "Electroosmotically driven microfluidic actuators," Sensors and Actuators B: Chemical 141(1), 263–269 (2009).

[25] Daghighi, Y., and Li, D., "Micro-valve using induced-charge electrokinetic motion of Janus particle.," Lab on a chip 11(17), 2929–40 (2011).

[26] Bau, H.H., Zhu, J., Qian, S., and Xiang, Y., "A magneto-hydrodynamically controlled fluidic network," Sensors and Actuators B: Chemical 88(2), 205–216 (2003).
[27] Álvarez-Barrientos, A., Arroyo, J., Cantón, R., Nombela, C., and Sánchez-Pérez, M., "Applications of Flow Cytometry to Clinical Microbiology," Clinical Microbiology Reviews 13(2), 167–195 (2000).
[28] Brown, M., and Wittwer, C., "Flow cytometry: Principles and clinical applications in hematology," Clinical Chemistry 46(8 B), 1221–1229 (2000).
[29] Watkins, N., Venkatesan, B.M., Toner, M., Rodriguez, W., and Bashir, R., "A robust electrical microcytometer with 3-dimensional hydrofocusing.," Lab on a chip 9(22), 3177–3184 (2009).
[30] Wolff, A., Perch-Nielsen, I.R., Larsen, U.D., Friis, P., Goranovic, G., Poulsen, C.R., Kutter, J.P., and Telleman, P., "Integrating advanced functionality in a microfabricated high-throughput fluorescent-activated cell sorter.," Lab on a chip 3(1), 22–27 (2003).
[31] Hashemi, N., Erickson, J.S., Golden, J.P., and Ligler, F.S., "Optofluidic characterization of marine algae using a microflow cytometer.," Biomicrofluidics 5(3), 32009–320099 (2011).
[32] Kekäläinen, J., Larma, I., Linden, M., and Evans, J.P., "Lectin staining and flow cytometry reveals female-induced sperm acrosome reaction and surface carbohydrate reorganization," Scientific Reports 5(October), 15321 (2015).
[33] Testa, G., Persichetti, G., and Bernini, R., "Micro flow cytometer with self-aligned 3D hydrodynamic focusing," Biomedical Optics Express 6(1), 54 (2014).
[34] Mao, X., Waldeisen, J.R., and Huang, T.J., "'Microfluidic drifting'--implementing three-dimensional hydrodynamic focusing with a single-layer planar microfluidic device.," Lab on a chip 7(10), 1260–1262 (2007).
[35] Mao, X., Lin, S.-C.S., Dong, C., and Huang, T.J., "Single-layer planar on-chip flow cytometer using microfluidic drifting based three-dimensional (3D) hydrodynamic focusing.," Lab on a chip 9(11), 1583–1589 (2009).
[36] Mao, X., Nawaz, A.A., Lin, S.-C.S., Lapsley, M.I., Zhao, Y., McCoy, J.P., El-Deiry, W.S., and Huang, T.J., "An integrated, multiparametric flow cytometry chip using 'microfluidic drifting' based three-dimensional hydrodynamic focusing.," Biomicrofluidics 6(2), 24113–241139 (2012).
[37] Nawaz, A.A., Nissly, R.H., Li, P., Shariff, Y.M., Wang, L., and Huang, T.J., "Differential Analysis of Lysed Whole Blood Via ' Microfluidic Drifting ' Based Flow Cytometry Chip" 1, 1068–1070 (2014).
[38] Nawaz, A.A., Nissly, R.H., Li, P., Chen, Y., Guo, F., Li, S., Shariff, Y.M., Qureshi, A.N., Wang, L., et al., "Immunological Analyses of Whole Blood via 'Microfluidic Drifting' Based Flow Cytometric Chip," Annals of Biomedical Engineering 42(11), 2303–2313 (2014).
[39] Nawaz, A.A., Zhang, X., Mao, X., Rufo, J., Lin, S.-C.S., Guo, F., Zhao, Y., Lapsley, M., Li, P., et al., "Sub-micrometer-precision, three-dimensional (3D) hydrodynamic focusing via 'microfluidic drifting,'" Lab Chip 14(2), 415–423 (2014).
[40] Bhagat, A.A.S., Kuntaegowdanahalli, S.S., and Papautsky, I., "Continuous particle separation in spiral microchannels using Dean flows and differential migration.," Lab on a chip 8(11), 1906–1914 (2008).
[41] Daghighi, Y., Sinn, I., Kopelman, R., and Li, D., "Experimental validation of induced-charge electrokinetic motion of electrically conducting particles," Electrochimica Acta 87, 270–276 (2013).
[42] Xia, Y., and Whitesides, G.M., "Soft Lithography" 28(12), 153–184 (1998).
[43] Daghighi, Y., "Microfluidic Technology and its Biomedical Applications," Journal of Thermal Engineering 1(7), 621–626 (2015).